# Thermoelectric Behavior of Organic Thin Film Nanocomposites

**Gregory P. Moriarty,[1] Sukanta De,[2] Paul J. King,[2] Umar Khan,[2] Michael Via,[3] Julia A. King,[3] Jonathan N. Coleman,[2] Jaime C. Grunlan[1]**

[1]Department of Mechanical Engineering, Texas A&M University, College Station, Texas 77843

[2]Department of Physics, Trinity College Dublin, Dublin 2, Ireland

[3]Department of Chemical Engineering, Michigan Technological University, Houghton, Michigan 49931

Correspondence to: J. C. Grunlan (E-mail: jgrunlan@tamu.edu)

Received 5 July 2012; revised 14 September 2012; accepted 14 September 2012; published online 16 October 2012
**DOI: 10.1002/polb.23186**

**ABSTRACT**: Organic thin film nanocomposites, prepared by liquid-phase exfoliation, were investigated for their superior electrical properties and thermoelectric behavior. Single-walled carbon nanotubes (SWNT) were stabilized by intrinsically conductive poly(3,4-ethylenedioxythiophene):poly(styrene sulfonate) (PEDOT:PSS) in an aqueous solution. The electrical conductivity ($\sigma$) was found to increase linearly as 20 to 95 wt % SWNT. At 95 wt % SWNT, these thin films exhibit metallic electrical conductivity ($\sim 4.0 \times 10^5$ S m$^{-1}$) that is among the highest values ever reported for a free-standing, fully organic material. The thermopower ($S$) remains relatively unaltered as the electrical conductivity increases, leading to a maximum power factor ($S^2\sigma$) of 140 $\mu$W m$^{-1}$ K$^{-2}$. This power factor is within an order of magnitude of bismuth telluride, so it is believed that these flexible films could be used for some unique thermoelectric applications requiring mechanical flexibility and printability. © 2012 Wiley Periodicals, Inc.† J Polym Sci Part B: Polym Phys 51: 119–123, 2013

**KEYWORDS**: carbon nanotubes; PEDOT:PSS; polymer thermoelectric; power factor; thermal conductivity

**INTRODUCTION** As the world continues to produce more power each year,[1] the energy that is dissipated into the environment as waste heat becomes more important as an alternative fuel source.[2,3] Thermoelectric materials have the ability to generate electricity from a small temperature gradient that is often created by inefficient power sources (e.g., combustion engines or power plants).[2,4–6] These materials make use of the Seebeck effect (opposite of the Peltier effect), in which an electric current is created through the diffusion of charge carriers, such as electrons or holes, from the hot side of the material to the cold, or vice versa. This movement of charge carriers then generates a voltage that can be harnessed to power various devices. This special class of materials is capable of improving the efficiency of any power generating system. Thermoelectric modules are robust, require no moving parts, and emit no sound. These qualities, along with high power density, which can be more than an order higher than traditional diesel generators,[7] make these materials ideal for compact mobile power sources or energy scavengers attached to inefficient systems. The thermoelectric figure of merit (ZT) is the most common measure of a material's energy conversion efficiency:

$$\mathrm{ZT} = \frac{\sigma S^2 \mathrm{T}}{\kappa} \tag{1}$$

where $S$ (V K$^{-1}$) is the thermopower (or Seebeck coefficient), $\sigma$ (S m$^{-1}$) is the electrical conductivity, $\kappa$ (W m$^{-1}$ K$^{-1}$) is the thermal conductivity, and $T$ (K) is the absolute measurement temperature.[8] A simpler value related to thermoelectric efficiency, known as the power factor ($S^2\sigma$), is often used to compare materials to one other.[6]

Recent developments in inorganic alloy materials have made this class of materials prevalent in commercial thermoelectric devices.[4] These alloys generally contain semiconductors, which have the best combination of properties to achieve a good ZT. Bismuth telluride ($Bi_2Te_3$) and its derivatives have been shown to achieve ZT values above 1 at room temperature,[4,9–15] which corresponds to ~8% of the Carnot efficiency.[16] It should be noted that a standard refrigerator operates at ~30% Carnot efficiency, which would require a thermoelectric material having a ZT of 4.[17] Unfortunately, these semiconductor alloys contain rare and expensive elements, are difficult to process, and have toxicity issues.[9–13,18] Organic materials have recently emerged as lower cost, more environmentally friendly alternatives to these semiconductor alloys.[7,19–31]

In the present work, organic thin film nanocomposites, prepared by liquid-phase exfoliation, were examined. Single-walled carbon nanotubes (SWNT) were stabilized by

intrinsically conductive poly(3,4-ethylenedioxythiophene): poly(styrene sulfonate) (PEDOT:PSS). It is shown that the electrical conductivity is increased from 50,000 to 4,00,000 S $m^{-1}$ as the SWNT concentration increased. The thermal conductivity and thermopower remain relatively unaffected with this large increase in electrical conductivity. Power factors of these thin films nanocomposites reach a maximum of 140 $\mu$W $m^{-1}$ $K^{-2}$ at 85 wt % SWNT. The ability of a completely organic material to reach metallic electrical conductivity is an important tool for many diverse applications.

## EXPERIMENTAL

### Materials and Preparation

Single-walled carbon nanotube (arc-discharge SWNT purchased from Iljin Nanotech Co., Seoul, Korea) dispersions were prepared by adding the nanotubes to a 10-mL cylindrical vial containing an aqueous solution of 5 $mgmL^{-1}$ PEDOT:PSS (Baytron PH500, purchased from H.C. Stark), such that the nanotube concentration was 1 $mgmL^{-1}$. This dispersion was subjected to 5 min of high-power tip sonication (VibraCell CVX, 750 W, 20% amplitude, 60 kHz) before being placed in a sonic bath (Branson 2510-MT) for 1 h and subjected to another 5 min of high-power sonication. These dispersions were blended in the ratio required to give the desired SWNT/PEDOT:PSS mass fraction. The mixtures were then sonicated for 15 min in a sonic bath to homogenize. The resulting dispersions were vacuum-filtered using 0.45 $\mu$m polyvinylidene fluoride (PVDF) filter membranes (MF-Millipore membrane, 47-mm diameter) to produce thick films. The thickness of these films was controlled by the volume of dispersion filtered and hence the deposited mass. Deposited films were washed with 200 mL of deionized water, dried under vacuum for 24 h at 60 °C, and peeled from the filter membrane to give a robust free standing film.

### Film Characterization

To measure the in-plane electrical conductivity and Seebeck coefficients, samples were cut into a rectangular shape ($\sim$15 mm in length and 2 mm in width) and measured with a home-built, shielded four-point probe apparatus, equipped with a Keithley 2000 Multimeter (Cleveland, OH) and a GW PPS-3635 power supply (Good Will Instrument Co.) and operated with a Labview (National Instruments, Austin, TX) interface. The resistances were extracted from the current–voltage ($I$–$V$) measurement as 0 to $\pm$ 1 mA was passed to the sample. Resistivity values were obtained by multiplying the slope of the linear $I$–$V$ curve by an averaged width and thickness of the sample, divided by the average distance between the two inner probes. Electrical conductivity values are then calculated by taking the inverse of the resistivity. Averages of the geometrical factors of the sample were obtained by three unique measurements to achieve the most accurate results possible. Seebeck coefficient measurements were obtained from the slope of a linear temperature voltage ($T$–$V$) curve as voltages across the sample were measured at eight different temperature gradients, each varying by $\pm$ 8 K. It should be noted that the coefficient of determination ($R^2$) for finding the slope of the $T$–$V$ measurement was greater than 0.99. The scanning electron micrographs of composite cross-sections were taken with an FEI Quanta 600 FE-SEM (Hillsboro, OR). Samples were soaked in liquid nitrogen and freeze fractured by hand. During imaging, the accelerating voltage was 10 kV, with a spot size of 3.0 nm and a working distance of $\sim$10 nm.

Thermal conductivity at 25 °C was measured with a Netzsch Instruments. Nanoflash LFA 447 in accordance with ASTM E1461-07. For a single through-plane thermal conductivity measurement, a 25.4-mm diameter disk (cut from the center of the thin film composites) was placed in the device. A Xenon flash lamp was then used to direct a short heat pulse of 10 J to the front side of the sample, as the temperature rise on the back surface of the disk was recorded as a function of time. For each sample, five separate heat pulses were used and the resulting thermal conductivities for each test were averaged. Furthermore, for each SWNT concentration, at least three thin films were measured. Specific heats were measured with a Q20 differential scanning calorimeter (DSC) (TA Instruments, New Castle, DE) in conjunction with ASTM E1269-05. The temperature was ramped at a rate of 20 °C $min^{-1}$, from $-60$ to 60 °C, during testing. To ensure accurate results, three tests were done for each sample. The heat flows of a sapphire standard ($D_{st}$) and loaded pan ($D_s$) were subtracted from an empty pan to cancel out the pan influence. The specific heat was then calculated using:

$$C_{p,s} = C_{p,st}\frac{D_s W_{st}}{D_{st} W_s} \quad (2)$$

where $W_{st}$ is the weight of the sapphire standard, $W_s$ is the weight of sample, and the resulting data were extrapolated to 25 °C.

## RESULTS AND DISCUSSION

### Composite Microstructure

In this work, SWNT was combined with the intrinsically conductive surfactant, PEDOT:PSS, to create organic thermoelectric thin films. PEDOT:PSS has been previously shown to effectively disperse carbon nanotubes (CNTs) in an aqueous solution and increase the electrical conductivity of the mixture as a whole.[19,32] Figure 1(a) depicts an exfoliated solution of CNT with PEDOT:PSS attached to its surface. The surfactant helps prevent the hydrophobic CNT from aggregating together through enhanced hydrophilicity. As the solution is allowed to dry, electrically conductive junctions form between CNT [Fig. 1(b)], which is believed to be the source of exceptional electronic properties.[33] These junctions are easily influenced by the interparticle distance, contact potential barriers, and electronic states of CNT but can be tailored by stabilizer type and concentration.[19,24]

Figure 1(c) shows a freeze-fractured cross-sectional SEM micrograph of a thin film made of 20 wt % SWNT and 80 wt % PEDOT:PSS. The bright spaghetti-like strands that appear here are nanotubes that have pulled out of the darker PEDOT:PSS matrix. At higher magnification [Fig. 1(d)], designated by the dotted-line box in Figure 1(c), PEDOT:PSS at

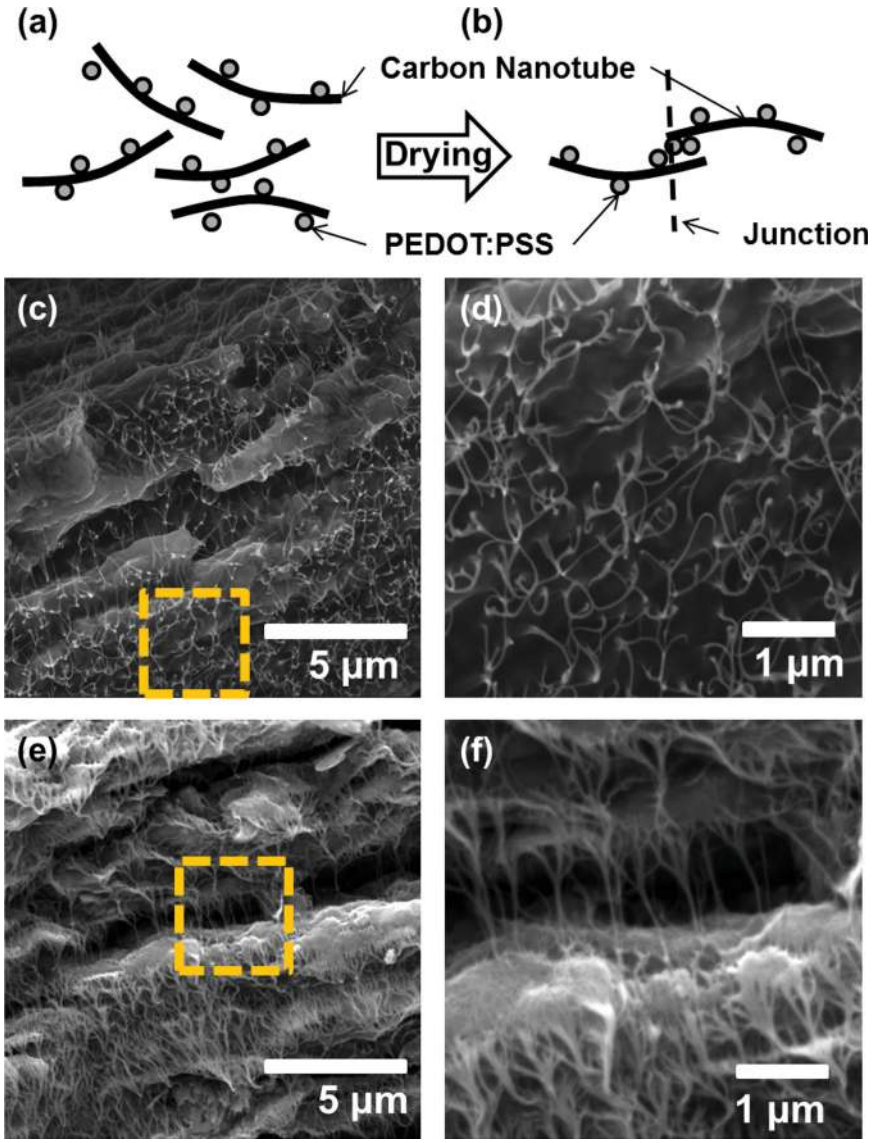


**FIGURE 1** Schematics of CNTs coated by PEDOT:PSS particles in their exfoliated state (a) and an electrically conductive junction formed between CNTs upon drying of the exfoliated solution (b). SEM cross-sectional images of a 20 wt % SWNT film (c) and a 60 wt % SWNT film (e). Images (d) and (f) are higher magnification images, marked by dotted boxes in (c) and (e), respectively. The balance of each film is PEDOT:PSS.

SWNT junctions are more clearly seen as brighter spots. These junctions are believed to impart metal-like electrical conductivity to the thin films. As the SWNT concentration is increased to 60 wt % [Fig. 1(e, f)], porosity within the microstructure is shown to increase as well. These microvoids are formed by the SWNT aggregation that increases as the PEDOT:PSS concentration is reduced. This porosity will affect the mechanical and transport properties of these thin films.

### Transport Properties

Table 1 summarizes the through-thickness thermal conductivity for the SWNT-filled thin films. These measurements were obtained using the transient method (ASTM E1461-07), where thermal conductivity ($\kappa$) is calculated from experimentally measured diffusivity ($\alpha$), specific heat ($C_p$), and density ($\rho$):

$$\kappa = \alpha \cdot C_p \cdot \rho \tag{3}$$

**TABLE 1** Thermal Properties of SWNT-PEDOT:PSS Thin Films

| SWNT Concentration (wt %) | Density (g cm$^{-3}$) | Specific Heat (J g$^{-1}$ K$^{-1}$) | Thermal Conductivity (W m$^{-1}$ K$^{-1}$) |
|---|---|---|---|
| 20 | 0.970 | 1.714 | 0.560 ± 0.068 |
| 40 | 1.171 | 1.503 | 0.444 ± 0.031 |
| 60 | 0.910 | 1.309 | 0.638 ± 0.290 |
| 77.5 | 0.610 | 1.183 | 0.687 ± 0.005 |
| 85 | 0.685 | 0.960 | 0.664 ± 0.008 |
| 95 | 0.636 | 0.956 | 0.526 ± 0.046 |

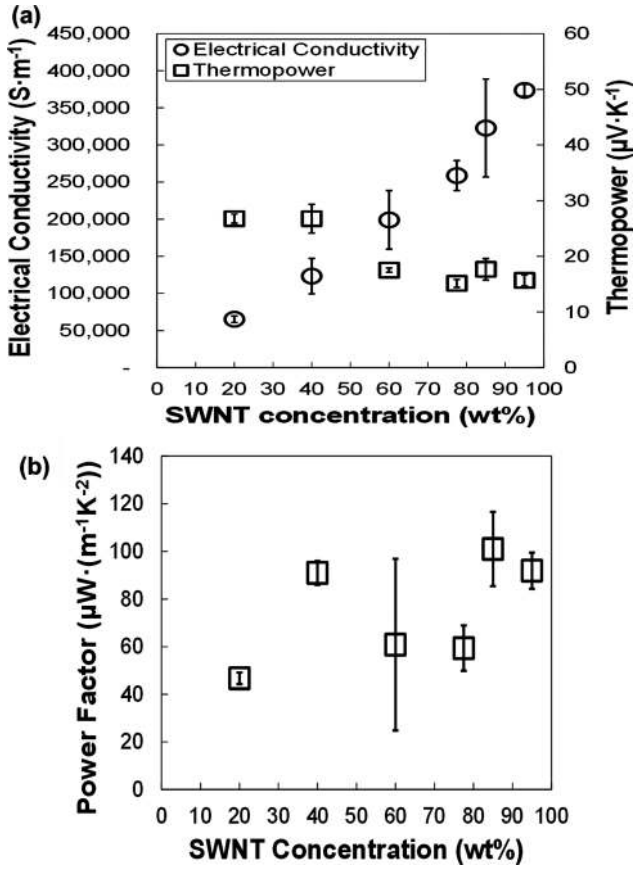


**FIGURE 2** Electrical conductivity, thermopower (a) and power factor (b) of SWNT/PEDOT:PSS thin films as a function of nanotube concentration.

As expected, the specific heat decreases with increasing SWNT concentration. These data agree with a simple rule of mixtures calculation, which is conceptually accurate because it would take less energy to raise the temperature as more conductive filler is introduced. These thin films have a slightly elevated polymer-like thermal conductivity (~0.4 W $m^{-1}$ $K^{-1}$),[7,19,24] ranging from 0.4 to 0.7 W $m^{-1}$ $K^{-1}$, despite displaying metal-like electrical conductivity [Fig. 2(a)]. A significant increase in the thermal conductivity would have been expected as the SWNT concentration increased because of the difference in conductivity between the PEDOT:PSS (~0.2 W $m^{-1}$ $K^{-1}$)[34] and that of the SWNTs (~1000 W $m^{-1}$ $K^{-1}$).[7,35] At 95 wt % SWNT, the thermal conductivity for the composite could have been as large as ~950 W $m^{-1}$ $K^{-1}$, based upon a simple rule of mixtures, but the low experimental values (0.53 W $m^{-1}$ $K^{-1}$ for the 95 wt % SWNT) can be attributed to the numerous high thermal contact resistances and differing vibrational frequencies occurring between the nanotubes and PEDOT:PSS (i.e., the Kapitza resistance).[19,24,36–40] This low $\kappa$ is also linked to increased porosity that accompanies the increase in SWNT concentration and further disrupts phonon transport through the film.[19,24]

Figure 2(a) shows the electrical conductivity and thermopower as a function of SWNT concentration for these thin films. Electrical conductivity appears to increase linearly with SWNT concentration. The highest conductivity of ~4.0 $\times$ $10^5$ S $m^{-1}$, obtained with 95 wt % SWNT, is orders of magnitude greater than previously reported values for other organic composite systems.[19,25,26,33,36] This high conductivity is attributed to the SWNT having an intrinsically high electrical conductivity, due to its highly conductive $\pi$-conjugated pathways that promote electron transport.[19,36] Additionally, PEDOT:PSS enhances the electrical conductivity of the thin films by creating less resistive tube—tube junctions.[19,36] As electrical conductivity of these composites is significantly altered by increasing SWNT concentration, the thermopower remains relatively unaltered (~14–26 $\mu$V $K^{-1}$) [Fig. 2(a)]. A small energy barrier is believed to hinder the transport of low-energy electrons (i.e., low-energy charge carriers) across the tube junctions, leaving the thermopower insensitive to changes in electrical conductivity and effectively decoupling these two properties.[7,19,36,41,42] This energy barrier for electron transport can be influenced by changing the stabilizer used to exfoliate the SWNT,[43] the interparticle distance,[44] the contact potential barrier,[44] and the electrostatic charges associate with the CNTs and matrix.[45,46] While the indirect contact of SWNT, and the weak bonding between SWNT—PEDOT:PSS at the junctions, effectively impede phonon transport, electrical conductivity can be maintained without direct contact between SWNT through hopping and tunneling of the energetic electrons.[41,46] These thin films display the general behavior of traditional semiconductors in a very weak sense, showing a slight reduction in thermopower with increasing electrical conductivity.[2,4–6]

The high electrical conductivity exhibited by these thin films results in above average power factors ($S^2\sigma$) commonly reported for all organic systems.[7,19,24–26,36] These values are roughly an order of magnitude lower than state-of-the-art inorganic materials[7,8] and are similar to other inorganic thin films.[25,26] Figure 2(b) shows that power factors do not show a distinct trend as the SWNT concentration is increased due to the large variability in electrical conductivity and slight deviations in thermopower measurements. However, a thin film composed of 85 wt % SWNT achieves a power factor of ~140 $\mu$W $m^{-1}$ $K^{-2}$, which is competitive with other types of good organic thermoelectric materials.[7,19,24,36] A calculated ZT value of ~0.03, from the power factor and through-plane thermal conductivity at 300 K for a 40 wt % SWNT film, makes these fully organic thin films viable for converting waste heat into useful electricity.

## CONCLUSIONS

These fully organic, water-processable and flexible thin films have many advantageous properties for thermoelectric applications. It has been demonstrated that SWNTs can be easily exfoliated with PEDOT:PSS and dried into thin, coherent films. These films can achieve among the highest reported electrical conductivity for an all organic system (~4.0 $\times$ $10^5$ S $m^{-1}$), while still maintaining a thermal conductivity similar to a heat insulating polymer (0.4–0.7 W $m^{-1}$ $K^{-1}$). A thin film composed of 85 wt % SWNT achieves a power factor of

$\sim$140 $\mu W\ m^{-1}\ K^{-2}$, which is competitive with other types of good organic thermoelectric materials. These results present a method to produce thin organic films for applications in thermoelectric devices or as metallic replacements. More work is underway to further improve the waste heat conversion efficiency of these thin films (i.e., produce greater ZT).


## ACKNOWLEDGMENTS

The FE-SEM acquisition was supported by the NSF grant DBI-0116835, the VP for Research Office, and the TX Eng. Exp. Station. The authors thank the US Air Force of Scientific Research (Grant No. FA9550-09-1-0609), under the auspices of Charles Lee, and the II–VI Foundation for financial support of this work.


## REFERENCES AND NOTES


**1** International Energy Outlook 2011. U.S. Energy Information Administration. DOE/EIA-0484; **2011**. www.eia.gov/ieo.

**2** Tritt, T. M.; Boettner, H.; Chen, L. *MRS Bull.* **2008**, *33*, 366–368.

**3** Chen, G.; Dresselhaus, M. S.; Dresselhaus, G.; Fleurial, J. P.; Caillat, T. *Int. Mater. Rev.* **2003**, *48*, 45–66.

**4** Snyder, J.; Toberer, E. S. *Nat. Mater.* **2008**, *7*, 105–114.

**5** Majumdar, A. *Science* **2004**, *303*, 777–778.

**6** Tritt, T. M.; Subramanian, M. A. *MRS Bull.* **2006**, *31*, 188–194.

**7** Kim, Y. S.; Kim, D.; Yu, C.; Grunlan, J. C. *Nano Lett.* **2008**, *8*, 4428–4432.

**8** Rowe, D. M. In Handbook of Thermoelectrics; CRC Press: Boca Raton, FL, **1995**.

**9** Harman, T. C.; Taylor, P. J.; Walsh, M. P.; LaForge, B. E. *Science* **2002**, *297*, 2229–2232.

**10** Venkatasubramanian, R.; Siivola, E.; Colpitts, T.; O'Quinn, B. *Nature* **2001**, *413*, 597–602.

**11** Hsu, K. F.; Loo, S.; Guo, F.; Chen, W.; Dyck, J. S.; Uher, C.; Hogan, T.; Polychroniadis, E. K.; Kanatzidis, M. G. *Science* **2004**, *303*, 818–821.

**12** Poudel, B.; Hao, Q.; Ma, Y.; Lan, Y. C.; Minnich, A.; Yu, B.; Yan, X.; Wang, D. Z.; Muto, A.; Vashaee, D.; Chen, X. Y.; Liu, J. M.; Dresselhaus, M. S.; Chen, G.; Ren, Z. *Science* **2008**, *320*, 634–638.

**13** Winters, J. *Mech. Eng.* **2008**, *130*, 30–33.

**14** Gothard, N. W.; Tritt, T. M.; Spowart, J. E. *J. Appl. Phys.* **2011**, *110*, 023706.

**15** Mehta, R. J.; Zhang, Y.; Karthik, C.; Singh, B.; Siegel, R. W.; Borca-Tasciuc, T.; Ramanath, G. *Nat. Mater.* **2012**, *11*, 233–240.

**16** Goldsmid, G. J. In 17th Int. Conf. on Thermoelectrics, Institute of Electrical and Electronics Engineers, Inc. Piscataway, NJ, **1998**; pp 25–28.

**17** DiSalvo, F. J. *Science* **1999**, *285*, 703–706.

**18** Winder, E. J.; Ellis, A. B.; Lisensky, G. C. *J. Chem. Educ.* **1996**, *73*, 940–946.

**19** Kim, D.; Kim, Y. S.; Choi, K.; Grunlan, J. C.; Yu, C. *ACS Nano* **2010**, *4*, 513–523.

**20** Yoshino, K.; Morita, S.; Yin, X. H.; Onoda, M. *Synth. Met.* **1993**, *55–57*, 3562–3565.

**21** Jousseaume, V.; Morsli, M.; Bonnet, A.; Tesson, O.; Lefrant, S. *J. Appl. Polym. Sci.* **1998**, *67*, 1205–1208.

**22** Hewitt, C. A.; Kaiser, A. B.; Roth, S.; Craps, M.; Czerw, R.; Carroll, D. L. *Nano Lett.* **2012**, *12*, 1307–1310.

**23** Levesque, I.; Gao, X.; Klug, D. D.; Tse, J. S.; Ratcliffe, C. I.; Leclerc, M. *React. Funct. Polym.* **2005**, *65*, 23–36.

**24** Moriarty, G. P.; Wheeler, J. N.; Yu, C.; Grunlan, J. C. *Carbon* **2012**, *50*, 885–895.

**25** Coleman, J. N.; Lotya, M.; O'Neill, A.; Bergin, S. D.; King, P. J.; Khan, U.; Young, K.; Gaucher, A.; De, S.; Smith, R. J.; Shvets, I. V.; Arora, S. K.; Stanton, G.; Kim, H.-Y.; Lee, K.; Kim, G. T.; Duesberg, G. S.; Hallam, T.; Boland, J. J.; Wang, J. J.; Donegan, J. F.; Grunlan, J. C.; Moriarty, G. P.; Shmeliov, A.; Nicholls, R. J.; Perkins, J. M.; Grieveson, E. M.; Theuwissen, K.; McComb, D. W.; Nellist, P. D.; Nicolosi, V. *Science* **2011**, *331*, 568–571.

**26** Smith, R. J.; King, P. J.; Lotya, M.; Wirtz, C.; Khan, U.; De, S.; O'Neill, A.; Duesberg, G. S.; Grunlan, J. C.; Moriarty, G. P.; Chen, J.; Wang, J.; Minett, A. I.; Nicolosi, V.; Coleman, J. N. *Adv. Mater.* **2011**, *23*, 3944–3948.

**27** Soon, J. M.; Loh, K. P. *Electrochem. Solid State Lett.* **2007**, *10*, A250–A254.

**28** Feng, C. Q.; Ma, J.; Li, H.; Zeng, R.; Guo, Z. P.; Liu, H. K. *Mater. Res. Bull.* **2009**, *44*, 1811–1815.

**29** Hernandez, Y.; Nicolosi, V.; Lotya, M.; Blighe, F. M.; Sun, Z.; De, S.; McGovern, I. T.; Holland, B.; Byrne, M.; Gun'Ko, Y. K.; Boland, J. J.; Niraj, P.; Duesberg, G.; Krishnamurthy, S.; Goodhue, R.; Hutichison, J.; Scardaci, V.; Ferrari, A. C.; Coleman, J. N. *Nat. Nanotechnol.* **2008**, *3*, 563–568.

**30** Wilson, J. A.; Yoffe, A. D. *Adv. Phys.* **1969**, *18*, 193–335.

**31** Osada, M.; Sasaki, T. *J. Mater. Chem.* **2009**, *19*, 2503–2511.

**32** Hermant, M. C.; Klumperman, B. A.; Kyrylyuk, V.; van der Schoot, P.; Koning, C. E. *Soft Matter* **2009**, *5*, 878–885.

**33** De, S.; Lyons, P. E.; Sorel, S.; Doherty, E. M.; King, P. J.; Blau, W. J.; Nirmalraj, P. N.; Boland, J. J.; Scardaci, V.; Joimel, J.; Coleman, J. N. *ACS Nano* **2009**, *3*, 714–720.

**34** Jiang, F.-X.; Xu, J.-K.; Lu, B.-Y.; Xie, Y.; Huang, R.-J.; Li, L.-F. *Chin. Phys. Lett.* **2008**, *25*, 2202–2205.

**35** Che, J.; Cagin, T. W.; Goddard, A. *Nanotechnology* **2000**, *11*, 65–69.

**36** Yu, C.; Choi, K.; Yin, L.; Grunlan, J. C. *ACS Nano* **2011**, *5*, 7885–7892.

**37** Huxtable, S. T.; Cahill, D. G.; Shenogin, S.; Xue, L.; Ozisik, R.; Barone, P.; Usrey, M.; Strano, M. S.; Siddons, G.; Shim, M.; Keblinski, P. *Nat. Mater.* **2003**, *11*, 731–734.

**38** Shenogin, S.; Xue, L.; Ozisik, R.; Keblinski, P.; Cahill, D. G. *J. Appl. Phys.* **2004**, *95*, 8136–8144.

**39** Hu, M.; Keblinski, P.; Wang, J.-S.; Raravikar, N. *J. Appl. Phys.* **2008**, *104*, 083503.

**40** Pollack, G. L. *Rev. Mod. Phys.* **1969**, *41*, 48–81.

**41** Kim, Y. S.; Kim, D.; Martin, K. J.; Yu, C.; Grunlan, J. C. *Macromol. Mater. Eng.* **2010**, *295*, 431–436.

**42** Scarola, V. W.; Mahan, G. D. *Phys. Rev. B* **2002**, *66*, 205405.

**43** Vaisman, L.; Wagner, H. D.; Marom G. *Adv. Colloid Interface Sci.* **2006**, *2*, 37–46.

**44** Balberg, I.; Azulay, D.; Toker, D.; Millo, O. *Int. J. Mod. Phys. B* **2004**, *18*, 2091–2121.

**45** Emmanuel, K.; Gehan, A. J. A. *J. Appl. Phys.* **2006**, *99*, 084302:1–7.

**46** Hermant, M. C.; Klumperman, B.; Kyrylyuk, A. V.; van der Schoot, P.; Koning C. E. *Soft Matter* **2009**, *5*, 878–885.